Ultra-fast multiple tunnelling of electromagnetic X-waves

2000 J. Phys. A: Math. Gen. 33 8559

(http://iopscience.iop.org/0305-4470/33/47/316)

J. Phys. A: Math. Gen. **33** (2000) 8559–8576. Printed in the UK PII: S0305-4470(00)17066-0

Ultra-fast multiple tunnelling of electromagnetic X-waves

Amr M Shaarawi†§ and Ioannis M Besieris‡

† Physics Department, American University in Cairo, PO Box 2511, Cairo 11511, Egypt
‡ Bradley Department of Electrical and Computer Engineering, Virginia Polytechnic Institute and State University, Blacksburg, VA 24061, USA

Received 12 September 2000

Abstract. A study is provided of the transmission of a three-dimensional electromagnetic X-wave undergoing frustrated total internal reflection on the upper surface of a multi-layered structure. The stratified structure consists of successive layers alternately allowing the transmission of evanescent and free-propagation components. It is shown that the peak of an X-wave is transmitted through these successive layers at an ultra-fast speed. Under certain conditions, the total traversal time through all successive evanescent and free-propagation sections appears to be less than zero. The peak of the transmitted pulse emerges from the stack before the incident peak reaches the front surface of the stratified structure. Conditions for the materialization of this ultra-fast multiple tunnelling of pulses are pointed out and their consequences and limitations are discussed.

(Some figures in this article are in colour only in the electronic version; see `www.iop.org`)

1. Introduction

It has been demonstrated that classical electromagnetic pulses undergoing frustrated total internal reflection are partially transmitted through a single slab at ultra-fast speeds that appear to be superluminal [1–4]. This situation is similar to other cases pertaining to the transmission of pulses through undersized sections of waveguides or to photonic tunnelling through dielectric mirrors [5–20]. It is also analogous to results related to the Hartman effect predicted from solutions to Schrödinger's equation within the context of quantum tunnelling [21]. In the aforementioned situations, the traversal time associated with the transmission of the peak of the pulse through the barrier region saturates to a constant value as the thickness of the barrier increases [5–7, 21]. This causes the speed of the pulse tunnelling through the barrier to appear to be superluminal. Energy flow analysis has indicated that the peak of the transmitted pulse is not causally related to that of the incident one. Contributions to the peak of the tunnelled field arise primarily from the leading portion of the incident pulse [5, 6]. Consequently, the transmitted peak emerges from this leading portion of the field, which is not directly related to the portion containing the peak of the incident pulse. This reshaping of the field of the pulse is the reason for the apparent superluminal propagation through the tunnelling region.

There have been recent reports on the transmission of pulses through two barriers separated by a free-propagation region. In addition to the usual saturation of the traversal times in the two barrier regions, it has been shown that the traversal times of the pulses are also independent of the length of the free-propagation region separating them [22, 23]. This unanticipated

§ On leave from: Department of Engineering Physics and Mathematics, Faculty of Engineering, Cairo University, Giza 12211, Egypt.

0305-4470/00/478559+18$30.00

result leads to swift pulse transmissions that can be much faster than the speed of light. The aforementioned results are based on the simulation of the transmission of pulses through two undersized sections of a waveguide [22]. The predicted ultra-fast multiple tunnelling requires that the waveguide sections contain weak precursory fields before the arrival of the peak of the pulse. Another study of tunnelling through two successive barriers deals with the one-dimensional Schrödinger equation. In this case, ultra-fast multiple tunnelling has been confirmed by evaluating the phase time associated with deep barrier penetration [23]. The aim of this work is to demonstrate that three-dimensional X-waves [24–28] transmitted through a multi-layered structure exhibit the aforementioned ultra-fast multiple-tunnelling effect. We use this specific case to demonstrate the possible existence of limitations on the number of barriers and the widths of the regions of free-propagation separating them.

In an earlier work, we have demonstrated that X-wave tunnelling can be achieved by assigning angles of incidence to the spectral components of the pulse that are greater than the critical angle [4]. Furthermore, we have shown that the peak of the tunnelling X-wave appears to be transmitted through the slab at speeds greatly exceeding the speed of light. Our investigation has demonstrated that transmitted pulses are enlarged when compared with the incident ones [4]. In this work, we investigate the possibility of ultra-fast multiple tunnelling for X-waves going through a stratified structure consisting of successive layers alternately allowing the transmission of evanescent and free-propagation components. Using spectral synthesis, a simple analytical solution is obtained for the tunnelling of a three-dimensional X-wave through a stratified structure. In the current investigation, we are primarily interested in the study of the time taken by the peak of an X-wave to tunnel through the entire structure. No special attention is given to the reflected pulse or the fields generated inside the various layers. The plan of this work is to solve for the field of an X-wave transmitted through a multi-layered planar structure. This is done in section 2, where we consider the case of a normally incident X-wave for which all the spectral components undergo frustrated total internal reflection. In section 3, we present numerical simulations of different scenarios. The results and implications of this work are discussed in section 4.

2. Analysis

Consider an X-wave normally incident on a multi-layered structure which is schematically represented in figure 1. The apex angle of the conic surface defining the wavevectors associated with the spectral plane-wave components of the X-wave is chosen such that $\xi > \theta_c = \sin^{-1}(n_2/n_1)$, where $n_i = \sqrt{\varepsilon_i/\varepsilon_0}$ is the refractive index of medium $i = 1$ or 2. For propagation along the positive z-direction, transverse electric (TE) polarization of the plane-wave components of the X-wave is achieved by working with the following vector Hertzian potential [29]:

$$\vec{\Pi}_{TE}(\vec{r}, t) = \Psi(\vec{r}, t)\vec{u}_z. \tag{1a}$$

The electric field intensity can be readily obtained, namely

$$\vec{E}(\vec{r}, t) = -Z\vec{\nabla} \times \partial_{ct}\vec{\Pi}_{TE}(\vec{r}, t) \tag{1b}$$

where $Z = \sqrt{\mu_0/\varepsilon_1}$, assuming that the medium is non-magnetic. For an X-wave normally incident on the slab, the Hertzian potential is defined in terms of a fourfold Fourier superposition as

$$\Psi^{(i)}(\vec{r}, t) = \int_{R^1} \mathrm{d}(\omega/c_1) \int_{R^3} \mathrm{d}^3\vec{k}\, A(\vec{k}, \omega)\, \mathrm{e}^{-\mathrm{i}\omega t}\mathrm{e}^{+\mathrm{i}(k_x x + k_y y + k_z z)}\delta\left((\omega/c_1)^2 - k_x^2 - k_y^2 - k_z^2\right) \tag{2a}$$

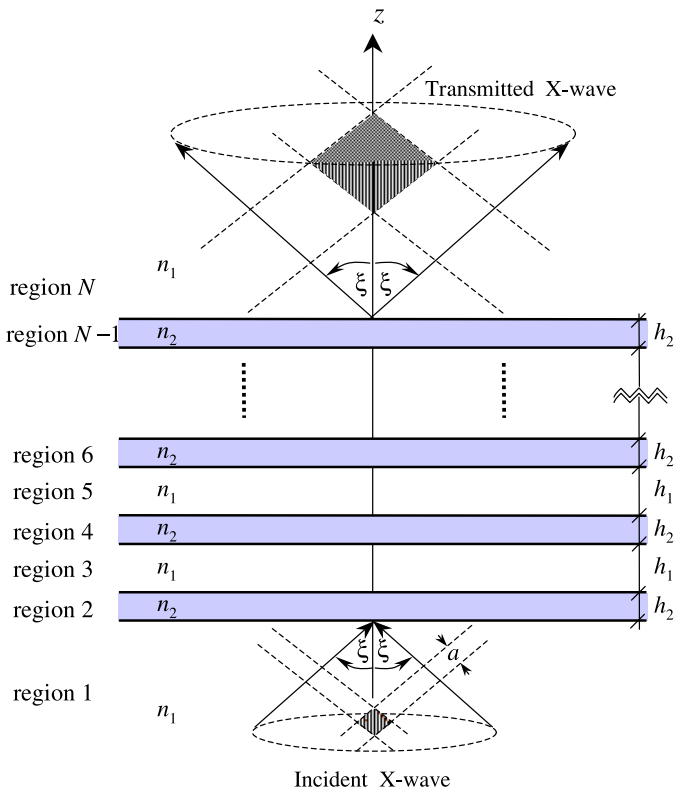

Figure 1. An X-wave incident normally on the upper surface of a multi-layered structure having $n_1 > n_2$.

where $c_1 = c_0/n_1$ is the wave speed in region 1 and the spectral amplitude is given by

$$A(\vec{k}, \omega) = \frac{1}{\pi}(\omega/\omega_0)^{\mu} \mathrm{e}^{-(\omega/c_1)a} \delta(k_z - (\omega/c_1)\cos\xi). \tag{2b}$$

The integrations in equation (2*a*) can be carried out explicitly to give the μth-order scalar X-wave solution; specifically,

$$\Psi^{(i)}(\vec{r}, t) = \frac{\Gamma(\mu+1)}{(\omega_0/c_1)^{\mu}\sqrt{\left(\rho^2\sin^2\xi + (a - \mathrm{i}(z\cos\xi - c_1 t))^2\right)^{\mu+1}}} \times F\left(\frac{\mu+1}{2}, -\frac{\mu}{2}, 1, \frac{\rho^2\sin^2\xi}{\rho^2\sin^2\xi + (a - \mathrm{i}(z\cos\xi - c_1 t))^2}\right). \tag{3}$$

Here, F is the hypergeometric function [30]. For integer values $\mu = m$. The above expression assumes the following form:

$$\Psi^{(i)}(\vec{r}, t) = (\omega_0/c_1)^{-m}\partial_a^m\left(\left[\rho^2\sin^2\xi + (a - \mathrm{i}(z\cos\xi - c_1 t))^2\right]^{-1/2}\right).$$

To determine the Hertzian potential associated with the transmitted field, one has to calculate the transmitted plane-wave components contributing to a Fourier superposition similar to that given in equation (2*a*). Considering the multi-layered structure shown in

figure 1, the spectral amplitudes of the incident and reflected fields in region 1 are related to the transmitted amplitudes in region N through the following matrix relationship [31]:

$$\begin{bmatrix} (A+R) \\ p_1(A-R)) \end{bmatrix} = \begin{bmatrix} \mathbb{I}_{11} & \mathbb{I}_{12} \\ \mathbb{I}_{21} & \mathbb{I}_{22} \end{bmatrix} \begin{bmatrix} T \\ p_N T \end{bmatrix} \tag{4}$$

where $[\mathbb{I}]$ is the matrix defining the transmission through the whole stratified structure and is given by the product of the characteristic matrices associated with all intermediate layers; specifically,

$$[\mathbb{I}] = [\mathbb{I}_2][\mathbb{I}_3]\cdots[\mathbb{I}_{N-1}]. \tag{5}$$

The characteristic matrix for each layer is defined by

$$[\mathbb{I}_i] = \begin{bmatrix} \cos\beta_i & -(\mathrm{i}/p_i)\sin\beta_i \\ \mathrm{i}p_i \sin\beta_i & \cos\beta_i \end{bmatrix} \tag{6a}$$

where

$$\beta_i = (\omega/c_0)n_i h_i \cos\theta_i \tag{6b}$$

$$p_i = n_i \cos\theta_i. \tag{6c}$$

Solving equation (4) to determine the transmitted amplitude in terms of the incident one, the following transmission coefficient is deduced [31]:

$$t(\vec{k},\omega) = \frac{T}{A} = \frac{2p_1}{(\mathbb{I}_{11}+\mathbb{I}_{12}p_N)p_1 + (\mathbb{I}_{21}+\mathbb{I}_{22}p_N)}. \tag{7}$$

For an X-wave incident on a multi-layered structure, the values of β_i and p_i depend on the refractive index and thickness of the ith layer in addition to the angle of incidence θ_i of the spectral components of the X-wave. One should note that the transmission coefficient given in equation (7) takes into consideration all the reflections inside the various layers. We choose the spectral angle ξ given in equation (2a) such that all components of the X-wave undergo total internal reflection when they pass from an optically denser layer to a less dense one. As shown in figure 1, we choose all odd layers to have the same refractive index n_1, while the even ones have refractive indices equal to n_2. For $n_1 > n_2$, an incident X-wave characterized by the axicon angle $\xi > \sin^{-1}(n_2/n_1)$ will undergo frustrated total internal reflections at the upper surfaces of the even-indexed layers. In these regions, the spectral amplitudes of the X-wave have evanescent z dependences. In the odd-indexed layers, we have propagating spectral components characterized by the angle $\theta_i = \xi$. Apart from the first and last regions, which are presumed to be semi-infinite, all odd (even) layers have the same thickness h_1 (h_2). For the stratified medium shown in figure 1, the β_i and p_i parameters given in equations (6a) and (6c) acquire the following explicit values for the odd-indexed layers:

$$\beta_{2\ell+1} = (\omega/c_0)n_1 h_1 \cos\xi \tag{8a}$$

$$p_{2\ell+1} = n_1 \cos\xi \tag{8b}$$

for $\ell = 1, 2, 3, \ldots, (N-1)/2$. As for the even-indexed layers, we have

$$\beta_{2\ell} = \mathrm{i}(\omega/c_0)n_2 h_2 \sqrt{n_{12}^2 \sin^2\xi - 1} \tag{8c}$$

$$p_{2\ell} = \mathrm{i}n_2 \sqrt{n_{12}^2 \sin^2\xi - 1} \tag{8d}$$

where $n_{12} = n_1/n_2$. Finally, the first and last regions have

$$p_1 = p_N = n_1 \cos\xi. \tag{8e}$$

The Hertzian potential associated with the transmitted field acquires the following form:

$$\Psi^{(t)}(\vec{r},t) = \int_{R^1} \mathrm{d}(\omega/c_1) \int_{R^3} \mathrm{d}^3\vec{k}\, t(\vec{k},\omega) A(\vec{k},\omega) \times \mathrm{e}^{-\mathrm{i}\omega t} \mathrm{e}^{+\mathrm{i}(k_x x + k_y y + k_z(z-d))} \delta\left((\omega/c_1)^2 - k_x^2 - k_y^2 - k_z^2\right). \tag{9}$$

The three integrations over $\mathrm{d}^3\vec{k}$ are carried out analytically to give

$$\Psi^{(t)}(\vec{r},t) = \int_0^\infty \mathrm{d}(\omega/c_1)(\omega/\omega_0)^\mu J_0((\omega/c_1)\rho\sin\xi)\, \mathrm{e}^{-(\omega/c_1)(a-\mathrm{i}(z\cos\xi - c_1 t))} \times \frac{2p_1 \mathrm{e}^{-\mathrm{i}(\omega/c_1)\{((N-3)/2)h_1 + ((N-1)/2)h_2\}\cos\xi}}{\mathbb{I}_{11}p_1 + \mathbb{I}_{12}p_1^2 + \mathbb{I}_{21} + \mathbb{I}_{22}p_1}. \tag{10}$$

In the next section, this integration is evaluated numerically to illustrate the behaviour of an X-wave tunnelling through a multi-layered structure. Specific examples are chosen to clarify the reasons for the occurrence of the ultra-fast transmission and its limitations.

3. Numerical results

In this section, we carry out several simulations of the behaviour of the transmitted field under various conditions. The aim of these simulations is to explain the phenomenon and to pinpoint the advantages and limitations of ultra-fast transmission using multi-layered structures. In particular, we would like to elucidate the differences between single- and multiple-barrier superluminal tunnelling. We start by illustrating certain aspects of deep barrier penetration, in particular, showing that the transmitted peak is generated before the incident pulse reaches the upper surface of the multi-layered structure. We proceed to show how adding more barriers can shift the peak of the pulse forward at the expense of decreasing its amplitude and localization. Furthermore, the ultra-fast transmission is examined for cases involving shallow barrier penetration. Finally, we present results pertaining to the effects of increasing the widths of the regions of free-propagation separating the various barriers.

3.1. Deep barrier penetration

In a previous study, we have considered the case of an X-wave tunnelling through a single slab [4]. Tunnelling was achieved by assigning angles of incidence for all spectral components of the X-wave that are larger than the critical angle at the upper interface of the slab. In our previous investigation, we have chosen to work with an incident X-wave having an ξ angle slightly larger than θ_c. Tunnelling under such a condition is referred to as shallow barrier penetration. In such a case, the position of the peak of the transmitted pulse z_m shows a distinct forward shift relative to the position z_0 of the peak of an X-wave travelling without a barrier. For the parameter values used in the aforementioned study, the forward shift $\Delta_1 = z_m - z_0$ was slightly less but almost equal to the width of the slab. This behaviour makes the peak of the pulse appear to have travelled through the barrier at a superluminal speed. For deep barrier penetration, when $\xi \gg \theta_c$, the ultra-fast transmission through a single barrier is more conspicuous. Under this condition, the forward shift $\Delta_1 = z_m - z_0$ can be much larger than the width of the barrier. The reason for this large forward displacement is that the peak of the transmitted pulse is formed in the precursory small-amplitude part of the field of the X-wave before the principal peak arrives at the barrier. This mechanism is very important for understanding the phenomenon of ultra-fast multiple tunnelling.

Consider the case of an X-wave normally incident on a single slab, for which $n_1 = 3$ and $n_2 = 1$. The X-wave is characterized by the unusually large apex angle $\xi = 85^\circ$ and the

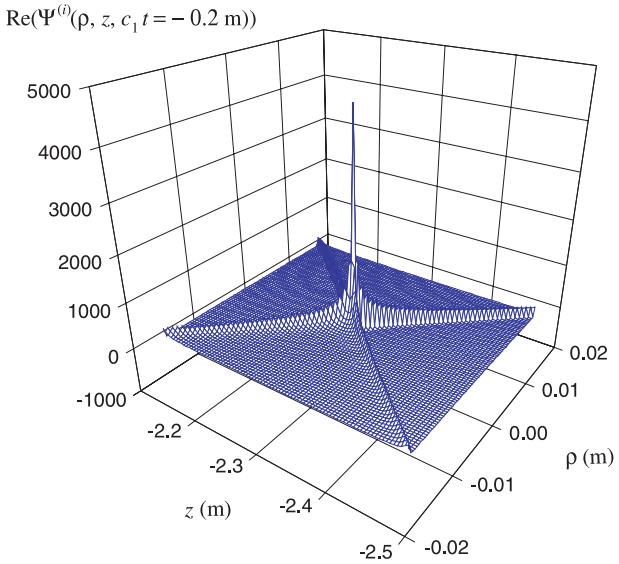

Figure 2. Surface plot of the Hertzian potential of the incident X-wave evaluated at $c_1 t = -200$ mm. The X-wave pulse has $a = 0.2$ mm, $\xi = 85^\circ$, $\mu = 0.25$ and $(\omega_0/c_1) = 5000\ \mathrm{m}^{-1}$.

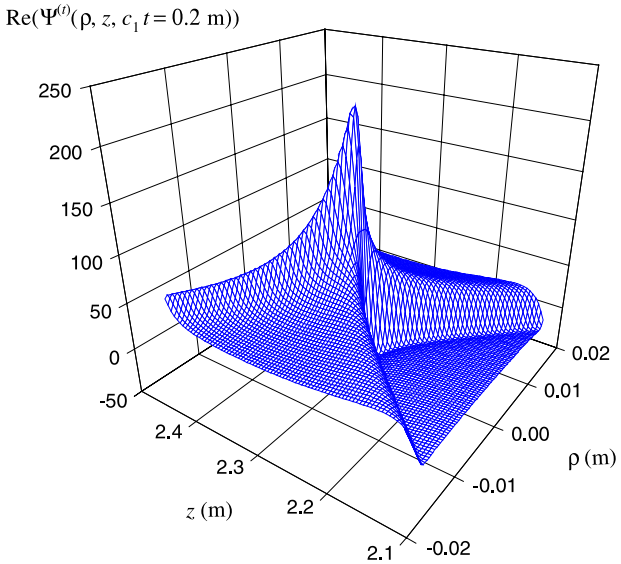

Figure 3. Surface plot of the Hertzian potential of the transmitted X-wave evaluated at $c_1 t = 200$ mm. The incident X-wave is the same one shown in figure 2. The slab width is $h_2 = 1$ mm and the refractive indices are $n_1 = 3$ and $n_2 = 1$.

parameter $a = 0.2$ mm. Note that having $\xi \gg \sin^{-1} n_{21} = 19.47^\circ$ ensures that all the Fourier plane-wave components of the X-wave undergo deep barrier penetration. As will be shown later on, the exaggerated large value of ξ has been chosen to emphasize certain aspects related to ultra-fast multiple tunnelling. In figure 2, a surface plot of the incident X-wave is provided at $ct = -200$ mm. The pulse shown has $a = 0.2$ mm, $\xi = 85^\circ$, $\mu = \frac{1}{4}$ and $(\omega_0/c_1) = 1/a$.

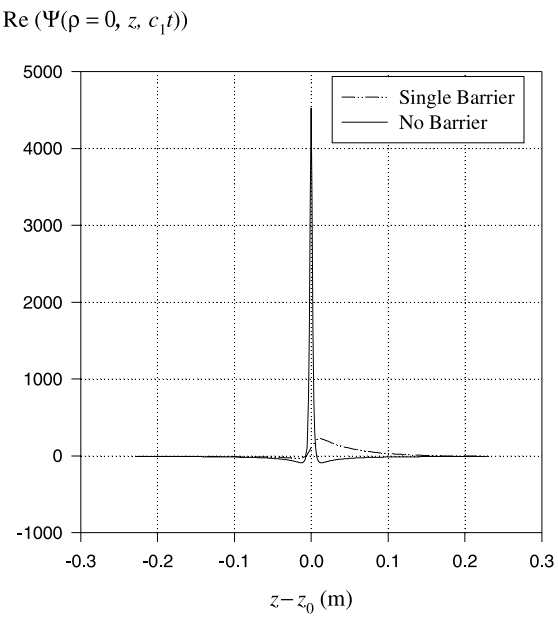

Figure 4. The axial profiles of the Hertzian potential of the transmitted X-wave for $h_2 = 0$ (full curve) and $h_2 = 1$ mm (broken curve). The two profiles were evaluated for an incident X-wave having $a = 0.2$ mm, $\xi = 85^\circ$, $\mu = 0.25$ and $(\omega_0/c_1) = 5000\ \mathrm{m}^{-1}$.

Unless explicitly stated that some parameter value has been changed, the X-wave shown in figure 2 is the one used as the incident pulse in all examples considered in this section. In figure 3, we display the pulse transmitted through a slab of width $h_2 = 1$ mm. The figure confirms the 'fattening' of the transmitted pulse as predicted in [4]. This 'fattened' pulse propagates in region 3 without any further spreading out, i.e. the transmitted pulse retains its non-dispersive character while propagating in region 3. Furthermore, one should note that the peak of the pulse is shifted forward relative to the rest of its field. In order to clarify this point, we compare in figure 4 plots of the axial profiles of the Hertzian potential of the transmitted pulses for $h_2 = 0$ and $h_2 = 1$ mm. The former corresponds to the case of having no slab or to that of an X-wave propagating freely in a medium having $n_1 = 3$. As can be seen from figure 4, the peak of the pulse transmitted through the slab is located in front of the peak of the pulse travelling in free-space. This behaviour is due to the reshaping of the pulse in the tunnelling region. The forward shift of the pulse transmitted through a single barrier $\Delta_1 = z_m - z_0 = 10.9\ \text{mm} \gg h_2$. To have a feeling of how fast the peak of the X-wave is transmitted through a single slab, we have plotted the difference $(z_m - z_0) - h_2$ for different values of h_2. Figure 5 shows that the difference $(z_m - z_0) - h_2$ acquires positive values and is much larger than h_2. This behaviour should be contrasted with cases having ξ slightly larger than θ_c. For the latter, the difference $(z_m - z_0) - h_2$ is negative and is much smaller than h_2 [4]. Large positive values of $(z_m - z_0) - h_2$ indicate that the forward shift is much larger than the width of the barrier. Given that the speed of the peak of the pulse is constant outside the barrier region, then the large forward shift means that an advanced pulse emerges into region 3 before the peak of the incident field reaches the barrier.

This advanced transmission of pulses due to deep barrier penetration begs the following question: how would deep barrier penetration affect the transmission of an X-wave pulse through two barriers separated by a distance h_1? Common wisdom suggests that the tunnelling

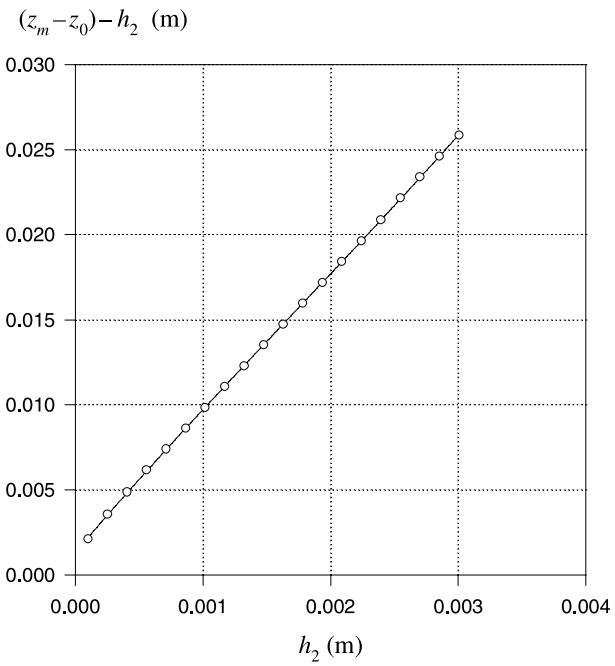

Figure 5. Plot of the difference $(z_m - z_0) - h_2$ versus h_2 for a pulse incident on a single barrier. The incident X-wave has the following parameter values: $a = 0.2$ mm, $\xi = 85^\circ$, $\mu = 0.25$ and $(\omega_0/c_1) = 5000$ m^{-1}. The positions of the peaks are calculated at $c_1 t = 200$ mm.

pulse is initially transmitted into region 3, then it propagates to the second barrier and tunnels through it, and finally a peak of the field emerges in region 5. For deep barrier penetration there is a slight complication; specifically, the transmitted pulse emerges from the tunnelling region before the peak of the incident field arrives at the first barrier. This happens when the principal peak is at a distance $\Delta_1 - h_2$ from the barrier. In what follows, we use the name advanced penetration length (ℓ_{ap}) to denote such distance. If the second barrier is separated from the first one by a propagation free region of width less than ℓ_{ap} (i.e. $h_1 < \Delta_1 - h_2$), then the pulse emerging from layer 2 will be at a distance that produces another advanced pulse in the region beyond the second barrier. The same effect can be reproduced *ad infinitum*, as more barriers are placed in the path of the X-wave while maintaining the condition $h_1 < \Delta_1 - h_2$. Consequently, the speed of transmission of the peak of the original pulse going through the whole stratified structure appears to be independent not only of the widths of the barriers, but also of the distances of free-propagation separating them [22, 23].

3.2. Effects of increasing the number of barriers

For the stratified structure shown in figure 1, we calculate the axial envelope of the field transmitted through a two-barrier structure having tunnelling regions of width equal to $h_2 = 1$ mm and that of the free-propagation layer equals $h_1 = 7$ mm. In figure 6, we display the incident and transmitted fields at $t = -7\cos\xi$ mm. In the figure, we have not shown the field reflected in region 1 because at this time instant the reflected field is negligibly small. Furthermore, adding the reflected field is a complication that will not affect the point illustrated by the figure. It is shown in figure 6 that the peak of the transmitted field exits

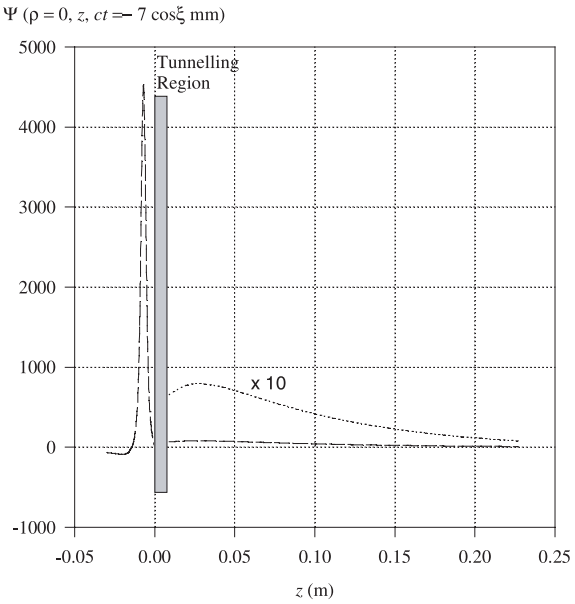

Figure 6. Advanced barrier penetration. The transmitted peak is formed before the incident pulse reaches the tunnelling structure. The incident X-wave has the same parameter values as in figure 2. The dotted curve represents the transmitted field magnified tenfold. The tunnelling structure consists of two barriers having widths $h_2 = 1$ mm and separated by a region of free propagation of width $h_1 = 7$ mm. The refractive indices of the different layers are equal to $n_1 = 3$ and $n_2 = 1$. The fields are calculated at $c_1 t = -7 \cos \xi$ mm.

Table 1. Forward shifts for one-, two- and three-barrier structures.

ξ	h_2 (mm)	h_1 (mm)	Δ_1 (mm)	Δ_2 (mm)	Δ_3 (mm)	d_1 (mm)	d_2 (mm)	d_3 (mm)
85°	1	7	10.90	34.421	58.515	1	9	17
75°	1	2	2.704	7.341	11.591	1	4	8
85°	2	—	19.505	—	—	2	—	—
	1	7	—	34.421	—	—	9	—
	$\frac{2}{3}$	7	—	—	43.6	—	—	16

the multi-layered structure before the incident pulse reaches the upper surface of the stack. This behaviour is responsible for the apparent superluminal transmission due to the multiple tunnelling of the X-wave.

In what follows, we investigate the possibility of adding extra barriers in order to achieve larger forward shifts. This is shown in figure 7, where the pulses transmitted from one, two and three barriers are plotted. The incident X-wave is the one shown in figure 2, the widths of the tunnelling regions equal $h_2 = 1$ mm and those of the free-propagation layers are $h_1 = 7$ mm. Figure 7 shows that the pulses undergo distinct forward shifts as the number of barriers is increased. However, the increase in the cumulative sum of the widths of the tunnelling regions ($2h_2$ or $3h_2$) results in a decrease of the amplitudes of the pulses and in the enlargement of their sizes. The forward shifts in the peaks of the pulses transmitted through the three configurations are denoted by Δ_n, where $n = 1, 2, 3$ indicates the number of barriers. The values of the forward shifts Δ_n for the three configurations are given in table 1. In the same table, the d_n

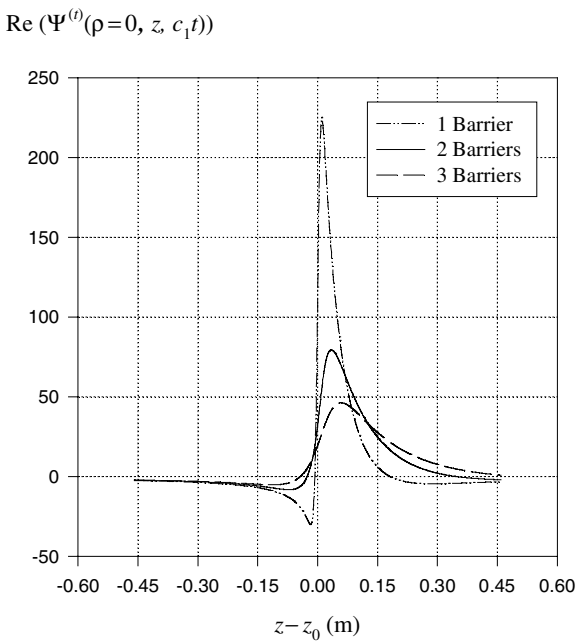

Figure 7. The axial profiles of the Hertzian potentials of the transmitted pulses for one-, two- and three-barrier configurations for which $h_2 = 1$ mm and $h_1 = 7$ mm. The three profiles were evaluated at $c_1 t = 200$ mm and the incident X-wave is characterized by the parameter values $a = 0.2$ mm, $\xi = 85^\circ$, $\mu = 0.25$ and $(\omega_0/c_1) = 5000\ \mathrm{m}^{-1}$. The refractive indices of the different layers are equal to $n_1 = 3$ and $n_2 = 1$.

values give the total width of the stratified structure for $n = 1, 2, 3$; i.e. the cumulative sum of the widths of all evanescent and free-propagation layers. For example, structures containing two or three barriers have $d_2 = h_1 + 2h_2$ or $d_3 = 2h_1 + 3h_2$, respectively. One should note that we have chosen h_1 to be less than ℓ_{ap}, where having $h_1 = 7\ \mathrm{mm} < (\Delta_1 - h_2) = 9.9$ mm satisfies the condition for advanced transmission of the pulses. It can be seen from table 1 that for a three-barrier structure, we have barrier widths $h_2 = 1$ mm separated by free-propagation layers each having $h_1 = 7$ mm. The cumulative sum of the widths of the three tunnelling regions is thus equal to $D = 3h_2 = 3$ mm. For this case, the forward shift in the position of the peak of the pulse equals $\Delta_3 = 58.51$ mm. This value should be compared with the forward shift of a single barrier having a width $D = h_2 = 3$ mm. As can be deduced from the plot provided in figure 5, the forward shift corresponding to the single barrier is $\Delta_1 \sim 29$ mm. This comparison demonstrates unequivocally the effectiveness of multiple tunnelling in producing large forward shifts in the peaks of the transmitted pulses. One should also note that for multiple tunnelling, the forward shift of the transmitted pulse Δ_n is much larger than the total width of the stratified structure d_n. In fact, table 1 indicates that for $\xi = 85^\circ$, a structure containing n barriers produces a forward shift having $\Delta_n > n\Delta_1 + d_n$.

3.3. Effects of shallow barrier penetration

To demonstrate the importance of deep barrier penetration on the phenomenon of ultra-fast transmission, we have calculated the forward shifts for an X-wave having $\xi = 75^\circ$. The envelopes of the axial fields for one-, two- and three-barrier configurations are shown in

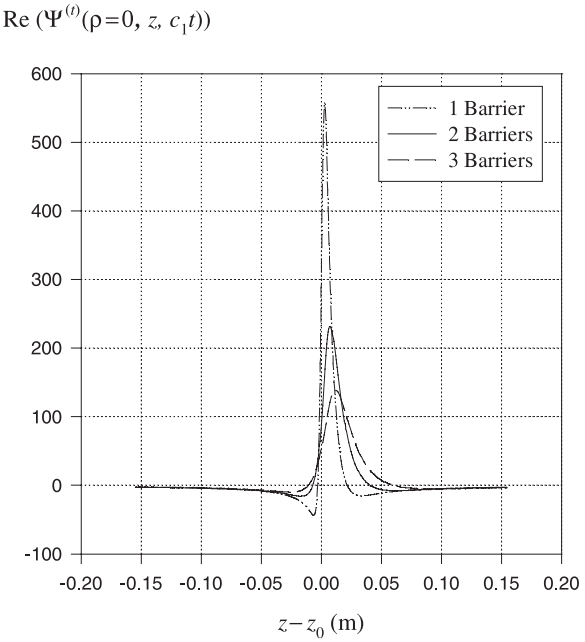

Figure 8. The axial profiles of the Hertzian potentials of the transmitted pulses for one-, two- and three-barrier configurations for which $h_2 = 1$ mm and $h_1 = 2$ mm. The three profiles were evaluated at $c_1t = 200$ mm and the incident X-wave is characterized by the parameter values $a = 0.2$ mm, $\xi = 75^\circ$, $\mu = 0.25$ and $(\omega_0/c_1) = 5000\ \mathrm{m}^{-1}$. The refractive indices of the different layers are equal to $n_1 = 3$ and $n_2 = 1$.

figure 8. The stratified structure is chosen to have $h_2 = 1$ and $h_1 = 2$ mm. The refractive indices of the different layers are $n_1 = 3$ and $n_2 = 1$. The values of the forward shifts Δ_n and the total widths of the stratified structures d_n are given in the second entry of table 1. One should note that the Hertzian potentials of pulses transmitted through a larger number of barriers show distinct forward shifts over pulses transmitted through a smaller number. For $\xi = 75^\circ$, the enlargement in the size of a transmitted X-wave is less than that occurring for a pulse having $\xi = 85^\circ$. Comparing the plots in figures 7 and 8, we see that the forward shifts for the smaller ξ angle are diminished significantly. Nevertheless, $\Delta_3 = 11.59$ mm is still larger than the forward shift resulting from a single barrier of width 3 mm for which $\Delta_1 = 7.92$ mm. To appreciate the need for deep barrier penetration in order to achieve ultra-fast multiple tunnelling, we provide plots of the difference $z_m - z_0 - D$ as a function of ξ. The two plots shown in figure 9 have tunnelling regions with equal cumulative widths. For a single barrier, we have $D = h_2 = 1$ mm, while for the two-barrier configuration the cumulative thickness of the tunnelling regions is $D = 2h_2 = 1$ mm. For the latter, the intermediate free-propagation region has $h_1 = 3$ mm. The figure shows that the two configurations have the same forward shifts up to angles $\xi < 55^\circ$. For larger angles, greater shifts are progressively observed in the position of the peak of the pulse transmitted through the two-barrier configuration.

3.4. Effects of increasing the widths of regions of free propagation

In this subsection, we would like to look at the case when the separations between the barriers are larger than ℓ_{ap}, i.e. $h_1 > \Delta_1 - h_2$. In figure 10, we display the axial envelopes

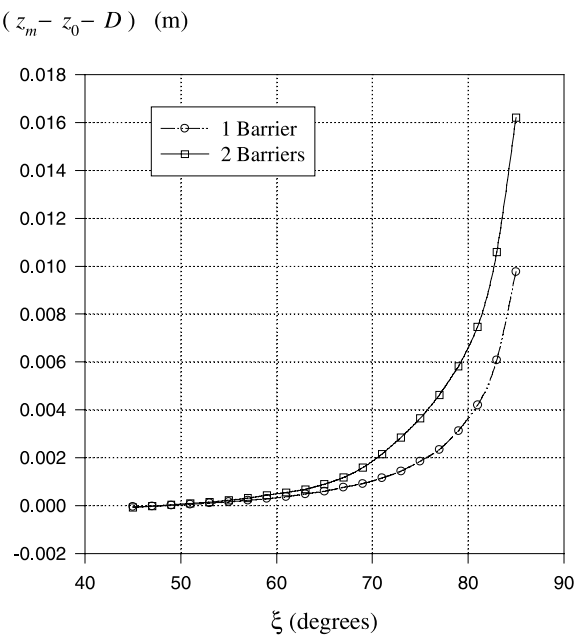

Figure 9. The dependence of the forward shift in the peak of the transmitted pulses on the apex angle ξ. For a single barrier $h_2 = 1$ mm, while for the two-barrier configuration $h_2 = 0.5$ and $h_1 = 3$ mm. The incident X-wave is characterized by the parameter values $a = 0.2$ mm, $\mu = 0.25$ and $(\omega_0/c_1) = 5000\ \mathrm{m}^{-1}$.

of the Hertzian potentials of three pulses transmitted by an X-wave having $\xi = 75^\circ$ incident on a two-barrier stack for which $h_2 = 1$ mm. The three plots are generated at $c_1 t = 200$ mm for barrier separation distances h_1 equal to 3, 6 and 60 mm. As can be seen from the plots, small-amplitude oscillations are introduced as h_1 becomes slightly larger than ℓ_{ap}. The observed ringing is generated due to the back-and-forth bouncing of the spectral components of the pulse in the intermediate region between the two barriers. For larger h_1 separations, spectral amplitudes tunnel through the second barrier after bouncing several times in the intermediate region. These transmitted components interfere both constructively and destructively causing the ringing in the transmitted field to become more pronounced. If the separation between the two barriers becomes large enough, then most spectral components interfere constructively to generate a train of delayed pulses. This can be seen for $h_1 = 60$ mm, where the separation between any two consecutive pulses equals $2h_1$, indicating that the delayed pulses have been transmitted after being bounced in the intermediate region an integer number of times. Apart from the ringing introduced as h_1 is enlarged, the increase in the forward shift of the pulse is limited. For the three separations $h_1 = 3$, 6 and 60 mm, the peak of the pulse acquires the forward shifts $\Delta_2 = 8.35$, 8.96 and 8.31 mm, respectively. This establishes that the largest forward shift for the peak of the tunnelling pulse is attained for barrier separation distances that are equal to ℓ_{ap}. For values $h_1 > \ell_{\mathrm{ap}}$, the forward shift for a given stratified structure saturates and does not vary significantly. Therefore, the optimal configuration for ultra-fast multiple tunnelling is to use barrier widths that produce forward shifts Δ_1 such that the separation distance between the barriers $h_1 \sim \ell_{\mathrm{ap}}$.

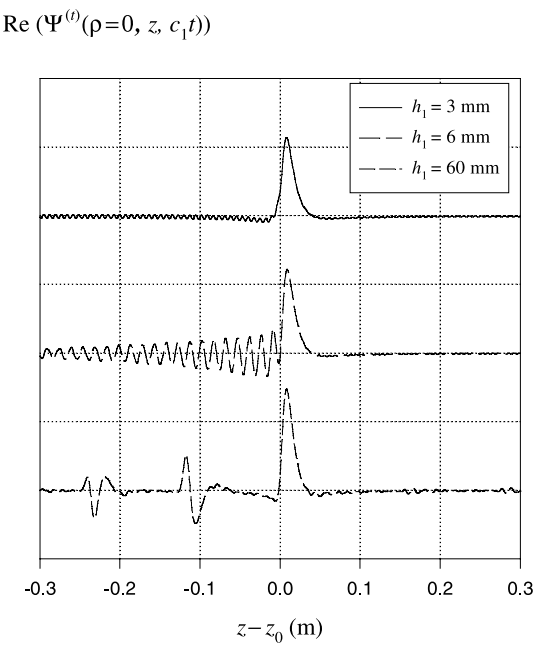

Figure 10. Profiles of the Hertzian potentials of pulses transmitted through a two-barrier configuration. The width of the tunnelling region is the same for the three configurations, where $h_2 = 1$ mm. Plots are provided for separation distances $h_1 = 3$, $h_1 = 6$ and $h_1 = 60$ mm. The forward shifts in the three cases equal $\Delta_2 = 8.54$, 8.96 and 8.31 mm. The incident X-waves have the same parameter values as in figure 8 and the refractive indices of the different layers are equal to $n_1 = 3$ and $n_2 = 1$.

3.5. Advantages of multiple-barrier tunnelling

One may argue that the forward shift due to multiple tunnelling can be obtained by tunnelling through a single barrier of a larger width. For example, consider the case of the first entry in table 1. For a two-barrier configuration with $h_2 = 1$ and $h_1 = 7$ mm, we obtain $\Delta_2 = 34.42$ mm. The same forward shift can be obtained using a single barrier of width $h_2 = 3.7$ mm. The Hertzian potentials of the pulses transmitted through these one- and two-barrier configurations are shown in figure 11. The wider tunnelling region of the single barrier results in a larger decay in the amplitude of the transmitted pulse. Furthermore, the pulse tunnelling through the two-barrier configuration is more localized. The plots shown in figure 11 illustrate the main advantage of multiple tunnelling, which is producing a large forward shift while transmitting a localized pulse that still has substantial amplitude. To emphasize this point, we have evaluated the axial envelope of an X-wave Hertzian potential transmitted through one-, two- and three-barrier configurations such that the cumulative width D is the same in the three cases. As such, we have chosen $h_2 = 2$, $h_2 = 1$ and $h_2 = \frac{2}{3}$ mm for one-, two- and three-barrier configurations, respectively. For the three cases, the cumulative barrier width is thus equal to $D = 2$ mm. The axial envelopes of the Hertzian potentials of the transmitted pulses are shown in figure 12. The plots demonstrate that the variations in the widths of the pulses are negligible. At the same time, the differences in their amplitudes are small. The forward shifts in the peaks of the pulses for the different configurations are supplied in the third entry in table 1. It is clear from the table that the three-barrier shift $\Delta_3 = 43.6$ mm is significantly larger than $\Delta_1 = 19.50$ mm for a single barrier. Our calculations thus indicate

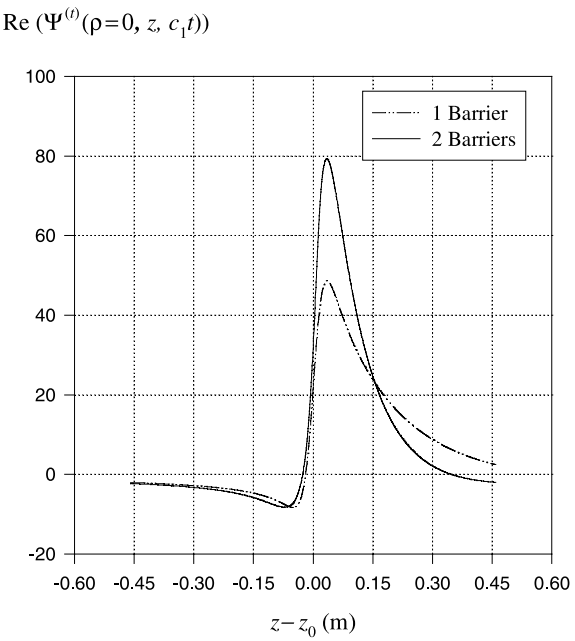

Figure 11. Two profiles of the Hertzian potentials of pulses transmitted through one- and two-barrier configurations such that their peaks have equal forward shifts $\Delta_1 = \Delta_2 = 34.4$ mm. The incident X-waves have the same parameter values as in figure 7. For the single barrier $h_2 = 3.7$ mm, while for the two-barrier configuration $h_2 = 1$ and $h_1 = 7$ mm.

that multiple tunnelling can produce large forward shifts in the position of the peak of the pulse without sacrificing too much amplitude or localization. This is the main advantage of the process of multiple tunnelling investigated in this work.

4. Concluding remarks

We have established that X-waves tunnelling through a stratified structure consisting of multiple barriers exhibit extraordinary waveform shaping that introduces large forward shifts in the peaks of the transmitted pulses. The peaks of the transmitted pulses appear to have moved through the stratified structure at ultra-fast speeds greatly exceeding the speed of light. Tunnelling is achieved by imposing the condition of total internal reflection on the Fourier spectral components of the X-waves. This is accomplished by choosing the spectral axicon angle ξ to be larger than the critical angle θ_c. It has been found that ultra-fast multiple tunnelling is intimately related to deep barrier penetration. For X-waves, deep barrier penetration is achieved when $\xi \gg \theta_c$. Under such a condition, ultra-fast transmission through a single barrier takes place because the peak of the transmitted pulse emerges from the tunnelling region before the peak of the incident pulse reaches the barrier. Understanding this non-local effect is essential when considering the phenomenon of ultra-fast tunnelling through a stack of multiple barriers.

In this paper, we have shown that multiple tunnelling can produce large forward shifts in the position of the peak of the transmitted pulse without losing too much amplitude or localization. A single barrier producing the same forward shift transmits a less localized pulse that suffers a larger decay in amplitude. The largest forward shift is obtained when the widths

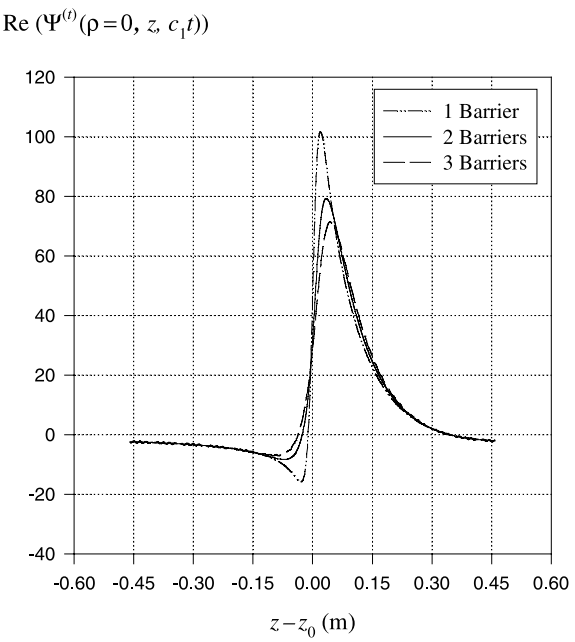

Figure 12. Profiles of the Hertzian potentials of pulses transmitted through one-, two- and three-barrier configurations. The cumulative sum of the widths of the tunnelling regions is the same for the three configurations, $D = 2$ mm. Specifically, $h_1 = 7$ mm while $h_2 = 2$, 1 and $\frac{2}{3}$ mm for one, two and three barriers, respectively. The incident X-waves have the same parameter values as in figure 7.

of the free-propagation regions h_1 are approximately equal to $\ell_{ap} = \Delta_1 - h_2$. Combining the condition $h_1 \sim \ell_{ap}$ with the deep penetration requirement $\xi \gg \theta_c$, we can produce forward shifts that are larger than the thickness of the whole stratified structure, i.e. larger than the sum of all tunnelling and free-propagation regions. Consequently, it appears that tunnelling through a stack consisting of many layers satisfying the condition $h_1 \sim \ell_{ap}$ should produce substantial forward shifts over extended distances. The results of this work are quite general and the same analysis is applicable to other pulses or beams whose spectral components have wavevectors confined to conic surfaces, e.g. focus-wave modes and Bessel beams [32–36]. Optical sources capable of generating X-waves, as well as other similar wave fields, have been reported [25, 35–38]. This makes it possible to test experimentally the predictions of the analysis presented in this work. Experimental difficulties can arise, however, due to the large ξ angle needed for the incident field and the finite size of the optical set-up.

Two factors limit the possibility of producing large forward shifts over extended distances. First, one should note that increasing the number of layers enlarges the cumulative width D of the tunnelling regions. A greater cumulative width introduces a larger decay in the amplitude of the transmitted pulse and a significant enlargement of its size. The second limiting factor is that the forward shift due to transmission through an n-barrier configuration saturates to a maximum value $(\Delta_n)_{max}$ as the separation between the barriers becomes greater than ℓ_{ap}. When h_1 is increased further, ringing appears on the transmitted pulse due to multiple reflections occurring in the free-propagation regions and no further increase in the forward shift is observed. These two effects impose practical constraints on achieving large forward shifts by tunnelling through a stratified medium. Since we are limited to separation distances satisfying the condition

$h_1 \sim \ell_{ap}$, any effective increase in the width of the stratified structure requires the addition of a large number of tunnelling layers. The latter causes the transmitted pulse to suffer larger amplitude loss and to become less localized. At this stage, the aforementioned limitations apply mainly to X-waves tunnelling through multi-layered planar structures. We cannot claim that the same factors are effective in other cases of interest, such as tunnelling through successive undersized sections in a waveguide filled with a precursory field [22]. Furthermore, the limiting factors pointed out here do not diminish the importance of the significant forward shift produced by multiple tunnelling.

At this stage, we would like to comment briefly on the origin of the superluminality of X-waves. It is well established that the speed of the peak of an X-wave travelling in free space is superluminal [24–27]. The parameters chosen in the examples used in section 3 give the following values for the velocity of the peak of the incident pulse: $v_1 = c_0/(n_1 \cos\xi) = 1.288c_0$ for $\xi = 75^\circ$ and $v_1 = 3.825c_0$ for 85°. The superluminality of the peaks of the X-waves arise from the interference of plane waves propagating along wavevectors lying on a conical surface [28]. The plane-wave components of the X-wave travel at the speed of light while the speed of their interference peak is superluminal. This superluminal speed is directly related to the apex angle of the cone. For multiple tunnelling, the position of the peak of the pulse is determined by the Fourier spectral components of the pulse interfering in the vicinity of the stratified structure. The transmitted peak appears to have moved through a distance larger than the thickness of the whole stack in zero time. Consequently, any estimate of the speed of transmission through the stratified structure would be much larger than the $1.288c_0$ and $3.825c_0$ values acquired initially by the incident pulse.

The results of this work confirm the established fact that the transmitted peak is created in a portion of the field that is different from that containing the incident peak. Nevertheless, the pulse would not have been transmitted in the first place if the extended field of the X-wave did not contain the incident peak. If the incident field contains two peaks, then the transmitted field produces two peaks. As such the incident pulses *cause* the transmitted peaks, although the two portions of the field are not *causally* related in the usual sense of special relativity. This classical *non-local causality* is similar to non-local phenomena arising within the context of quantum mechanics, e.g. the EPR paradox, non-locality of correlated states and single-particle interference effects. This point needs further study; specifically, one has to consider the effect of the enlargement of the sizes of the transmitted pulses on the possible loss of information incorporated in a sequence of incident pulses.

Finally, we would like to stress that this work is far from being exhaustive and that several unclear issues need to be explained in future studies. Mainly, we should understand the details of the temporal build-up of evanescent and propagation fields in the intermediate regions. We have to provide answers to a number of key questions before claiming to have a full understanding of the phenomenon. For example, while maintaining the condition $h_1 \sim \ell_{ap}$, does a tunnelling pulse treat the stratified structure as a single barrier and tunnels, in one shot, through the whole structure? Or, alternatively, do secondary peaks emerge at the various free-propagation sections simultaneously and subsequently each one of them tunnels through the succeeding barrier? Another point that needs to be clarified is how the evanescent fields inside the tunnelling regions mediate the transmission of pulses prior to the arrival of the original peaks at the barrier. Other studies should deal with the effect of tunnelling through structures with varying barrier widths. The possibility of limiting the enlargement of the sizes of the transmitted pulses using graded structures can be of interest in applications concerned with the transfer of information.

Acknowledgment

The authors wish to thank Professor Erasmo Recami, of Università degli Studi di Bergamo, Italy, for continuous scientific collaboration and a productive exchange of ideas. This work was motivated by preprints of [22, 23] that Professor Recami kindly passed to the first author.

References

[1] Ghatak A and Banerjee S 1989 Temporal delay of a pulse undergoing frustrated total internal reflection *Appl. Opt.* **28** 161–2
[2] Balcou Ph and Dutraix L 1997 Dual optical tunneling times in frustrated total internal reflection *Phys. Rev. Lett.* **78** 851–4
[3] Carey J J, Zawadzka J, Jaroszynski D J and Wynne K 2000 Noncausal time response in frustrated total internal reflection? *Phys. Rev. Lett.* **84** 1431–4
[4] Shaarawi A M and Besieris I M 2000 Superluminal tunneling of an electromagnetic X-wave through a planar slab *Phys. Rev.* E at press
[5] Hauge E H and Støvneng J A 1989 Tunneling times: a critical review *Rev. Mod. Phys.* **61** 917–36
[6] Martin Th and Landauer R 1992 Time delay of evanescent electromagnetic waves and the analogy to particle tunneling *Phys. Rev.* A **45** 2611–7
[7] Olkhovsky V S and Recami E 1992 Recent developments in the time analysis of tunneling processes *Phys. Rep.* **214** 339–56
[8] Nimtz G, Enders A and Spieker H 1994 Photonic tunneling times *J. Physique* I **4** 1–10
[9] Enders A and Nimtz G 1992 On superluminal barrier traversal *J. Physique* I **2** 1693–8
[10] Enders A and Nimtz G 1993 Evanescent-mode propagation and quantum tunneling *Phys. Rev.* E **48** 632–5
[11] Enders A and Nimtz G 1993 Zero-time tunneling of evanescent mode packets *J. Physique* **3** 1089–92
[12] Emig T 1996 Propagation of an electromagnetic pulse through waveguide with barrier: a time domain solution within classical electrodynamics *Phys. Rev.* E **54** 5780–7
[13] Dahmen H D, Gjonaj E and Stroh T 1998 Quantile motion of electromagnetic waves in wave guides of varying cross section and dispersive media *Ann. Phys., Lpz.* **7** 645–53
[14] Mugnai D, Ranfagni A, Ruggeri R, Agresti A and Recami E 1995 Superluminal processes and signal velocity in tunneling simulation *Phys. Lett.* A **209** 227–34
[15] Jakiel J, Olkhovsky V S and Recami E 1998 On superluminal motions in photon and particle tunnellings *Phys. Lett.* A **248** 156–60
[16] Steinberg A M, Kwiat P G and Chiao R Y 1993 Measurement of the single-photon tunneling time *Phys. Rev. Lett.* **71** 708–11
[17] Laude V and Tournois P 1999 Superluminal asymptotic tunneling times through one-dimensional photonic bandgaps in quarter-wave-stack dielectric mirrors *J. Opt. Soc. Am.* B **16** 194–8
[18] Martin Th and Landauer R 1992 Time delay of evanescent electromagnetic waves and the analogy to particle tunneling *Phys. Rev.* A **45** 2611–7
[19] Olkhovsky V S, Recami E, Raciti F and Zaichenko A K 1995 More about tunneling times, the dwell time and the Hartman effect *J. Physique* **5** 1351–65
[20] Ranfagni A, Mugnai D and Agresti A 1991 The role of the forerunner in the tunneling time determination *Phys. Lett.* A **158** 161–6
[21] Hartman T E 1962 Tunneling of a wave packet *J. Appl. Phys.* **33** 3427–33
[22] Barbero A P L, Hernández-Figueroa H E and Recami E 2000 On the propagation speed of evanescent modes *Phys. Rev.* E at press
(Barbero A P L, Hernández-Figueroa H E and Recami E 1998 *Preprint* ph/9811001)
[23] Olkhovsky V S, Recami E and Salesi G Tunneling through two successive barriers and the Hartman (superluminal) effect *Preprint*
[24] Lu J Y and Greenleaf J F 1992 Nondiffracting X waves—exact solutions to free space scalar wave equation and their finite aperture realization *IEEE Trans. Ultrasonic Ferroelec. Frequency Control* **39** 19–31
[25] Saari P and Reivelt K 1997 Evidence of X-shaped propagation-invariant localized light waves *Phys. Rev. Lett.* **21** 4135–8
[26] Besieris I M, Abdel-Rahman M, Shaarawi A and Chatzipetros A 1998 Two fundamental representations of localized pulse solutions of the scalar wave equation *Progr. Electromagn. Res. (PIER)* **19** 1–48
[27] Recami E 1998 On the localized X-shaped superluminal solutions to Maxwell's equations *Physica* A **252** 586–610

[28] Fagerholm J, Friberg A T, Huttunen J, Morgan D P and Salomaa M M 1996 Angular-spectrum representation of nondiffracting X waves *Phys. Rev.* E **54** 4347–52
[29] Stratton J A 1941 *Electromagnetic Theory* (New York: McGraw-Hill)
[30] Gradshteyn I S and Ryzhik I M 1965 *Tables of Integrals, Series and Products* (New York: Academic)
[31] Born M and Wolf E 1989 *Principles of Optics* (Oxford: Pergamon)
[32] Brittingham J N 1983 Focus wave modes in homogeneous Maxwell equations: transverse electric mode *J. Appl. Phys.* **54** 1179–89
[33] Ziolkowski R W 1985 Exact solutions of the wave equation with complex source locations *J. Math. Phys.* **26** 861–3
[34] Hillion P 1998 Electromagnetic tunneling Bessel beams *Opt. Commun.* **153** 199–201
[35] Saari P and Sõnajalg H 1997 Pulsed Bessel beams *Laser Phys.* **7** 32–9
[36] Durnin J, Miceli J J Jr and Eberly J H 1987 Diffraction free beams *Phys. Rev. Lett.* **58** 1499–501
[37] Turnen J, Vasara A and Friberg A T 1988 Holographic generation of diffraction-free beams *Appl. Opt.* **27** 3959–62
[38] Horvath Z L, Erdelyi M, Szabo G, Bor Zs, Tittel F K and Cavallaro J R 1997 Generation of nearly nondiffracting Bessel beams with a Fabry–Perot interferometer *J. Opt. Soc. Am.* A **14** 3009–13